Pertanika J. Sci. & Technol. 31 (6): 3059 - 3075 (2023)

PERTANIKA JOURNALS

SCIENCE & TECHNOLOGY

Journal homepage: http://www.pertanika.upm.edu.my/

Numerical Analysis and Validation of Characterization of Polydimethylsiloxane Using Hyper-elastic Constitutive Models

Sana Zulfiqar[1], Abdullah Aziz Saad[1]*, Zulkifli Ahmad[2], Feizal Yusof[1] and Zuraihana Bachok[1]

[1]School of Mechanical Engineering, Universiti Sains Malaysia, Nibong Tebal, 14300, Pulau Penang, Malaysia
[2]School of Materials & Mineral Resources Engineering, Universiti Sains Malaysia, Nibong Tebal, 14300, Pulau Penang, Malaysia

ABSTRACT

The most researched elastomer in recent years is polydimethylsiloxane (PDMS), which has several uses in various engineering industries. One of the PDMS's key characteristics is its hyper-elasticity nature, which enables the production of sensors, flexible electrical circuits, transducers, and antennas. This study used the hyper-elastic constitutive models to predict the mechanical behavior of incompressible, isotropic, and hyper-elastic material PDMS under uniaxial tension. These models are curve-fitting tools that consist of strain energy density and stress functions. To pursue the analysis, a new formulation of PDMS substrate was proposed, and a tensile test was performed to evaluate its stress-strain behavior. The experimental data was implemented on various hyper-elastic models using Abaqus, like Mooney-Rivlin, Yeoh, Ogden, and reduced polynomial models. The goodness of fit of every model was evaluated by calculating R^2 values. Consequently, among these models, the reduced polynomial model with 6 material constants possessed the highest R^2 value (0.9936) and was considered the best-fit model among the other models. Furthermore, the material constants of this model were applied to the 3D dumbbell-shaped model of PDMS in Abaqus for its validation. The boundary conditions were applied on the model similar to the experimental setup, as 33 mm displacement on one end and the other was fixed with all DOF. For mesh quality and mesh sensitivity of the material, various mesh sizes with the linear formulation (C3D8RH) were utilized, and the best mesh size was selected to evaluate very close results with the experimental.

Keywords: Characterization of material, FEM analysis, hyper-elastic material models, material parameters, polydimethylsiloxane

ARTICLE INFO

Article history:
Received: 16 November 2022
Accepted: 14 March 2023
Published: 09 October 2023

DOI: https://doi.org/10.47836/pjst.31.6.23

E-mail addresses:
zulfiqar.sana@ymail.com (Sana Zulfiqar)
azizsaad@usm.my (Abdullah Aziz Saad)
zulkifli@usm.my (Zulkifli Ahmad)
mefeizal@usm.my (Feizal Yusof)
zuraihana@usm.my (Zuraihana Bachok)
* Corresponding author

ISSN: 0128-7680
e-ISSN: 2231-8526

INTRODUCTION

Recently, the most popular building material of the siloxane family is polydimethylsiloxane (PDMS). Much work has been done on the applications of PDMS based on its several characteristics and properties like flexibility, elastomeric properties, high chemical resistivity, gas permeability, optical transparency (Izdihar et al., 2021; Martin & Bhushan, 2017), corrosion resistance, bio-compatible (Hassler et al., 2011), thermally stable and viscoelastic nature (Roh et al., 2016). It can easily mold into any shape and is cheaper than other elastomers. In addition, PDMS is non-toxic, non-flammable, and inert. It has a large variety of applications in mechanical, electrical, electronics and biomedical fields (Jewkes et al., 2018) such as stretchable electronic circuits (Zulfiqar et al., 2020; Zulfiqar et al., 2021), mechanical & electrochemical sensors (Casanova-Moreno et al., 2017), robotics, micro-fluid channels (Akther et al., 2020; Bashirzadeh et al., 2018) and Micro-electromechanical systems (MEMS)/Nano Electro-Mechanical System (NEMS) (Yu & Zhao, 2009).

PDMS, a rubber-like hyper-elastic material, is characterized by low elastic and high bulk modulus. The hyper-elastic materials possess large elastic strain and deformation under small volumetric changes. These materials are generally incompressible and do not obey Hooke's law, but they retain excellent energy absorption properties. The mechanical behavior of hyper-elastic materials can be characterized by implementing two methods: experimental and numerical simulation (Aziz et al., 2020; Íñiguez-Macedo et al., 2019; Sugihardjo et al., 2018; S Zulfiqar et al., 2022). Hence, several tests are available for the mechanical characterization of PDMS, such as tensile, fatigue, and creep tests (Doan & Mertiny, 2020; Martins et al., 2010).

Universal Tensile Machine (UTM) is used for different tensile tests. However, for rubber-like materials, ASTM D412 Type C standard (ASTM D412-16, 2021) is opted to make samples. The dog bone-shaped sample is fixed in the two holding grips of the machine in which one side is fixed, and the other is movable, having incremental displacement. This test's main objective is to determine a material's elastomeric properties. From this approach, the more realistic results with higher accuracy are obtained. On the other hand, using numerical software, like Abaqus, Ansys, and SolidWorks, has become more trending (Ribeiro et al., 2018; Souza et al., 2020; Xue et al., 2016). Several hyper-elastic material models for incompressible and isotropic materials, based on the experimental stress-strain data (uniaxial and biaxial) have been proposed in the last 80 years (Anssari-Benam & Bucchi, 2021; Beda, 2007; Bien-aimé et al., 2020; López-Campos et al., 2019; Nunes, 2011; Sattarian & Ghassemi, 2019; Tansel et al., 2020) that give better agreement with uniaxial tensile test data and pure shear data (Beda & Chevalier, 2003; Pucci & Saccomandi, 2002). The popular hyper-elastic material models based on classical Gaussian law (Boyce & Arruda, 2000; Meissner & Matějka, 2002; Wineman, 2005) are Neo-Hookean, Mooney-Rivlin, Yeoh, and Ogden models. The selection of these models depends on experimental

data and working strain range such as Neo-Hookean 30%, Mooney-Rivlin 30% compression & 200% tension, and Ogden up to 700% or more (Faghihi et al., 2014; Gonzalez et al., 2008; Kim et al., 2012; Yu & Zhao, 2009).

The main objective of this study is to characterize the mechanical behavior, in terms of modulus of elasticity and strength, of the proposed PDMS substrate by implementing uniaxial tensile test data on Mooney-Rivlin, Ogden, Yeoh, and reduced polynomial models. The uniaxial tensile test is done to calculate the elastic modulus and tensile strength of the PDMS substrate. Based on stress-strain experimental results, the most suitable constitutive model is selected to simulate the behavior of PDMS further. Finally, FEM analysis is carried out in Abaqus/CAE software to validate material characterization using the material parameters of selected hyper-elastic models on a 3D dumbbell-shaped model under the same boundary conditions used in uniaxial tensile testing. The accuracy of simulated results will be improved by mesh sensitivity and mesh quality analysis.

HYPER-ELASTIC CONSTITUTIVE MATERIAL MODELS

The mechanical behavior of hyper-elastic materials is calculated by FEM analysis. The accurate constitutive material model is selected to reproduce the non-linear hyper-elastic behavior of a material. The hyper-elastic models are categorized into two types of models: micro-mechanical and macro-mechanical models. Micro-mechanical models work on the methodology of unit cells and manufactured by using different chemicals, while on the other hand, macro-mechanical models study the material's behavior on an experimental data basis. The tensile test is very important for macro-mechanical models to get the experimental data.

Hyper-elastic material models determine the non-linear behavior of hyper-elastic materials like elastomers and rubbers. These models do not work under simple Hooke's law and have a non-linear stress-strain relationship. The hyper-elastic materials are considered to be isotropic and incompressible and have the capability to come to their original shape after unloading, and their flexibility is independent of strain rate (Ali et al., 2010). Such materials also have non-linear mechanical properties under high strain rates. The theory of hyper-elastic materials is defined as a function of strain energy or Helmholtz free energy. Helmholtz free energy measures the work output in the closed thermodynamics system under constant volume and temperature (Wriggers, 2008). The strain energy function plays a very important role in developing a hyper-elastic model by assuming different shapes based on the type of material used. It is also known as the stored energy function obtained by considering thermodynamics and symmetry (Wriggers, 2008). Mathematically, for isotropic and incompressible materials, the strain energy (W) function depending on three strain invariants is $W = f(I_1, I_2, I_3)$. The strain invariants in terms of principal stretches (λ) are given as Equations 1–3:

$$I_1 = {\lambda_1}^2 + {\lambda_2}^2 + {\lambda_3}^2 \quad [1]$$

$$I_2 = {\lambda_1}^2{\lambda_2}^2 + {\lambda_2}^2{\lambda_3}^2 + {\lambda_3}^2{\lambda_1}^2 \quad [2]$$

$$I_3 = {\lambda_1}^2{\lambda_2}^2{\lambda_3}^2 \quad [3]$$

For incompressible materials, the strain energy function can be written in terms of deviatoric strain energy (W_d) and volumetric (W_v) strain energy, as given in Equation 4. Hence, the general strain energy (W), stress (σ), and stretch ratio (λ) equations are expressed in Equations 5–7.

$$W = W_d(I_1, I_2) + W_V(J) \quad [4]$$

$$W = \sum_{i+j=1}^{N} C_{ij}(I_1 - 3)^i(I_2 - 3)^j + \sum_{k=1}^{N} \frac{1}{D_k}(J-1)^{2k} \quad [5]$$

$$\sigma = \lambda_i \frac{\delta W}{\delta \lambda_j} - pI \quad [6]$$

$$\lambda_i = 1 + \varepsilon_i = \left({L_i}/{L_o}\right)_i \quad [7]$$

Where J is the Jacobean determinant, C_{ij} and D_k are material constants. In the case of incompressible materials, $J = I_3 = \det F = 1$ and hydrostatic pressure (p) are negligible, so Equations 5 and 6 are reduced to Equations 8 and 9, respectively.

$$W = \sum_{i+j=1}^{N} C_{ij}(I_1 - 3)^i(I_2 - 3)^j \quad [8]$$

$$\sigma = \left[\frac{\delta W}{\delta I_1} + I_1 \frac{\delta W}{\delta I_2}\right] B - 2\frac{\delta W}{\delta I_2} B^2 \quad [9]$$

Further, the simple stress equation for hyper-elastic deformation behavior in uniaxial, equi-biaxial, and pure shear extension are expressed in Equations 10-12 (Bien-aimé et al., 2020). In case of uniaxial, $\lambda_2 = \lambda_3 = 1/\sqrt{\lambda}$.

$$\sigma_{uniax} = 2\left[{\lambda_1}^2 - \frac{1}{(\lambda_1\lambda_2)^2}\right]\left[\frac{\delta W}{\delta I_1} + {\lambda_2}^2\frac{\delta W}{\delta I_2}\right] \quad [10]$$

$$\sigma_{biax} = 2\left[{\lambda_2}^2 - \frac{1}{(\lambda_1\lambda_2)^2}\right]\left[\frac{\delta W}{\delta I_1} + {\lambda_1}^2\frac{\delta W}{\delta I_2}\right] \quad [11]$$

$$\sigma_{shear} = 0 \quad [12]$$

Mooney-Rivlin Model

Mooney-Rivlin model is a phenomenological type model that gives better convergence for a relatively large deformation rate than the Neo-Hookean model (Guo & Sluys, 2006). It is the extension of the Neo-Hookean model, which provides more accurate results. The Mooney-Rivlin model is limited to the uniaxial loading and does not work under biaxial or shear and complex loadings. This model has different forms based on the number of parameters, namely material constants. The selection of a number of parameters of this model depends on the type of stress-strain curve (Guo & Sluys, 2006). The general form of strain energy function (W) of the Mooney-Rivlin model is given in Equation 13, and the uniaxial stress (σ_{uniax}) with N number of material constants (C_{ij}) is defined in Equation 14 for incompressible materials.

$$W = \sum_{i,j=0}^{N} C_{ij} (I_1 - 3)^i (I_2 - 3)^j \quad [13]$$

$$\sigma_{uniax} = 2C_{10}\left(\lambda^2 - \frac{1}{\lambda}\right) + 2C_{01}\left(\lambda - \frac{1}{\lambda^2}\right) \quad [14]$$

Ogden Model

The Ogden material model is chosen to describe the non-linear behavior of complex materials like polymers, rubber, and tissues. It usually works under a larger deformation strain rate of up to 700%. The strain energy and uniaxial stress functions are generally expressed by Equations 15 and 16, respectively.

$$W = \sum_{i=1}^{N} \frac{\mu_i}{\alpha_i} (\lambda_1{}^{\alpha_i} + \lambda_2{}^{\alpha_i} + \lambda_3{}^{\alpha_i} - 3) \quad [15]$$

$$\sigma_{uniax} = \sum_{i=1}^{N} \mu_i \left(\lambda^{\alpha_i - 1} - \lambda^{-1/2\alpha_i - 1}\right) \quad [16]$$

Where W is the strain energy density function, N is the number of terms in series, λ_i (i = 1,2,3) is deviatoric principal stretches, μ_i, and α_i are temperature dependent material constants.

Yeoh Model

The most appropriate model used for incompressible materials is the Yeoh model because it only involves a third-order polynomial with I_1 dependence (first invariant deformation). It also produces more accurate results than the Neo-Hookean model due to its higher-order first invariant terms. However, it is very difficult to determine the dependence of Helmholtz energy on second or more invariant deformation terms. Therefore, Yeoh neglected I_2 and

higher-order terms. This model is also known as a reduced polynomial model (N=3), and for incompressible materials, the strain energy function and uniaxial stress can be expressed in Equations 17 and 18, respectively.

$$W = \sum_{i=1}^{N=3} C_{i0}(I_1 - 3)^i = C_{10}(I_1 - 3) + C_{20}(I_1 - 3)^2 + C_{30}(I_1 - 3)^3 \quad [17]$$

$$\sigma_{uniax} = 2[C_{10} + 2C_{20}(I_1 - 3) + 3C_{30}(I_1 - 3)^2] \quad [18]$$

Polynomial and Reduced Polynomial Model

A phenomenological model of rubber elasticity is the polynomial hyper-elastic material model. The elastic characteristics of compressible materials can also be described using this approach. It is also a general form of the Neo-Hookean, Mooney-Rivlin, and Yeoh hyper-elastic models and can be extended up to six orders. The polynomial model's strain energy density function is defined in Equation 5 (Ju et al., 2014). The strain energy equation becomes the Mooney-Rivlin model for $N-1$, and the incompressibility factor equals zero. However, if all the C_{ij} parameters are equal to zero except $j \neq 0$, then the final form of the polynomial hyper-elastic model is converted to a reduced polynomial hyper-elastic model. The strain energy equation is reduced to the general form of the Yeoh model (Equation 17). The respective uniaxial stress equation of this model is given in Equation 19.

$$\sigma_{uniax} = 2[C_{10} + 2C_{20}(I_1 - 3) + 3C_{30}(I_1 - 3)^2 + 4C_{40}(I_1 - 3)^3 + 5C_{50}(I_1 - 3)^4 6C_{60}(I_1 - 3)^5] \quad [19]$$

MATERIALS AND METHODS

Materials and Sample Preparation

The properties and functions of these materials are illustrated in Table 1: Poly(dimethylsiloxane) hydroxyl-terminated (PDMS-OH), fume silica, (3-glycidyloxypropyl) trimethoxysilane (ETMS), toluene, and dibutyltin dilaurate (DBDTL).

The substrate was prepared using PDMS-OH (hydroxyl terminated) as a base polymer and (3-glycidyloxypropyl) trimethoxysilane (ETMS) as cross–linking agent in a ratio of 33:1 (33 parts base polymer and 1 part cross-linking agent). The base polymer was mixed with a viscosity controller (fume silica) and solvent (toluene) for 30 minutes. After that, ETMS was added and mixed for the next 10 minutes. Finally, DBDTL catalyst was mixed into the solution to boost the reaction. The solution was then poured into a rectangular mold to get the rectangular-shaped sheet after curing for 24 hours at room temperature. The three samples of cured PDMS sheets were cut into dumbbell shapes of ASTM D412 Type C standard (Figure 1).

Table 1
Materials with their properties and functions

Materials	Function	Properties
PDMS-OH	Epoxy resin (binder)	Mol. wt.: 110×10^3 g/mol Viscosity: 50×10^3 cSt
Fume silica	Viscosity controller	Particle size: 5–50 nm Specific gravity: 2.2–2.3 g/ml
Toluene	Organic solvent	Mol. wt.: 92.14 g/mol Purity: 99% Density: 0.867 g/ml
ETMS	Cross-linking agent	Mol. wt.: 236.34 g/mol Purity: ≥ 98% Specific gravity: 1.07 g/ml
DBDTL	Catalyst	Mol. wt.: 631.56 g/mol Purity: 95% Density: 1.066 g/ml

EXPERIMENTAL AND CURVE FITTING OF HYPER-ELASTIC MODELS

Figure 1. PDMS sample based on ASTM D412 type C standard

PDMS samples were subjected to uniaxial tensile testing under a 10 mm/min loading rate and 10 kN load cell at room temperature. The test samples were gripped at the two ends with 33 mm length. The modulus of elasticity was obtained from the stress-strain curve at small strain values where stress is directly proportional to the strain (validate Hooke's law). Figure 2 shows the non-linear behavior of PDMS substrate in uniaxial tensile testing.

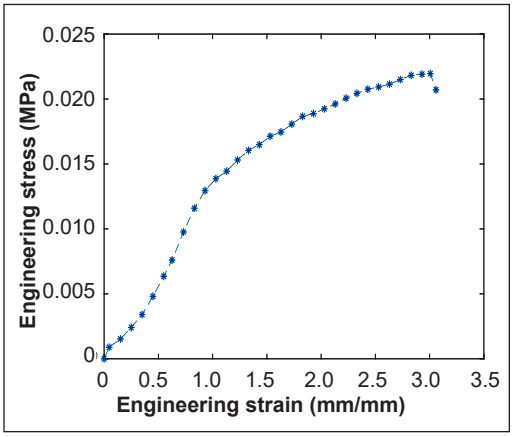

Figure 2. Engineering stress-strain curve of uniaxial tensile data of PDMS material

The engineering stress-strain data was introduced into Abaqus/CAE software to perform the FEM analysis and curve fitting of material (Ali et al., 2010; Subhani & Kumar, 2009) using different built-in hyper-elastic models such as Mooney-Rivlin, Yeoh, Ogden, and reduced polynomial. The curve fittings of all these models with respect to the experimental data are depicted in Figure 3. In addition, every hyper-elastic model's accuracy or goodness of fit was examined by coefficient of determination (R^2) values. For the best fit hyper-elastic model, the value of

R^2 must be obtained as 1 or very close to 1. However, the general formula for calculating R^2 is given in Equation 20.

$$R^2 = 1 - \frac{\sum_{i=1}^{n}\left(Y_{i,exp} - Y_{i,model}\right)^2}{\sum_{i=1}^{n}\left(Y_{i,exp} - \overline{Y_{i,exp}}\right)^2} \quad [20]$$

The parameters used in Equation 20 are defined as n is the total number of data points, I represent the integer values from 1 to n, Y_{exp} demotes the experimental stress values w.r.t. the stretch ratio (λ_{exp}), $\overline{Y_{exp}}$ is the average value of experimental stress data, and Y_{model} gives the stress values obtained by curve fitting of hyper-elastic model w.r.t. the stretch ratio (λ_{model}).

According to Figure 3, the reduced polynomial (N = 6) hyper-elastic model shows stability for all strain values and volumetric data, whereas the other hyper-elastic models are not stable under small and large deformations with the particular uniaxial tensile test data. Hence, the material coefficients and accuracy of respective hyper-elastic constitutive models obtained by curve fitting analysis are listed in Tables 2 and 3.

From Tables 2 and 3, it can be seen that the lowest coefficient of determination value (R^2), i.e., 0.8991, was obtained by using Mooney-Rivlin (N = 2), while the highest R^2 value using a reduced polynomial model with 6 number of material constants was calculated as 0.9963. This value explained the accuracy of the hyper-elastic model w.r.t. to the experimental test data. Thus, based on its accuracy and curve fitting graph, the reduced polynomial hyper-elastic model was selected as the best fit hyper-elastic model (Figure 3).

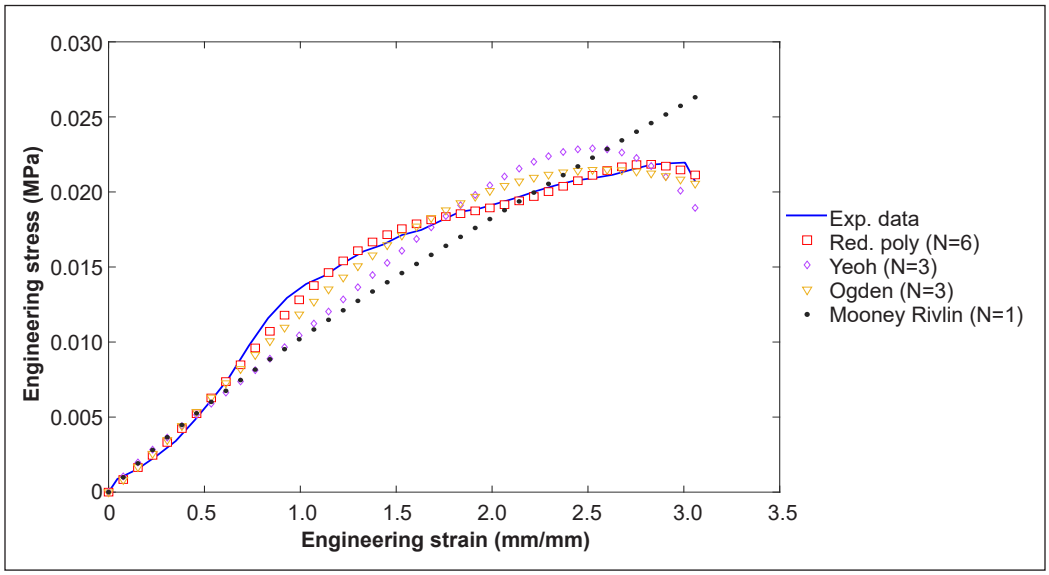

Figure 3. Curve fitting of experimental tensile data for PDMS material using different hyper-elastic constitutive models

Table 2
Material constants and accuracy of Mooney-Rivlin, Yeoh, and Reduced Polynomial models

FE Models	Material Constants [C_{ij}, MPa]							R_2
	C_{10}	C_{20}	C_{30}	C_{40}	C_{50}	C_{60}	C_{01}	
Mooney-Rivlin ($N = 1$)	3.65×10^{-3}	-	-	-	-	-	-1.44×10^{-3}	0.8991
Yeoh ($N = 3$)	2.45×10^{-3}	1.61×10^{-4}	-7.83×10^{-6}	-	-	-	-	0.9474
Reduced Polynomial ($N = 6$)	1.94×10^{-3}	8.20×10^{-4}	-1.65×10^{-4}	1.57×10^{-5}	-7.18×10^{-7}	1.28×10^{-8}	-	0.9963

Table 3
Material constants and accuracy of the Ogden model

FE Model	Material Constants						R^2
	μ_1 (MPa)	μ_2 (MPa)	μ_3 (MPa)	α_1	α_2	α_3	
Ogden ($N = 3$)	0.347	-0.149	-0.194	1.998	2.269	1.698	0.9814

NUMERICAL ANALYSIS AND VALIDATION OF BEST FIT HYPER-ELASTIC MODEL

In this study, the numerical analysis was simulated initially by considering only the elastic region of the specimen. The goal of employing PDMS' elastic characteristics in FEM simulation was to acquire strain values in the elastic area. A 3D dumbbell-shaped model based on the ASTM D412 type C standard was developed, as shown in Figure 4.

The material properties of PDMS were implemented on the above model. These properties include modulus of elasticity as 0.48 MPa and Poisson's ratio as 0.499. The material constants of reduced polynomial (N=6), such as $C_{10} = 0.00194$, $C_{20} = 0.00082$, $C_{30} = -0.000165$, $C_{40} = 1.57 \times 10^{-5}$, $C_{50} = -7.18 \times 10^{-7}$ and $C_{60} = 1.28 \times 10^{-8}$, were chosen based on its high accuracy value than the other hyper-elastic models. The element type 8-node linear brick, hybrid formulation, constant pressure, reduced integration, and hourglass control (C3D8RH) opted for meshing. After meshing, the boundary conditions, as per uniaxial tensile testing, were set as all degree of freedom (DOF) was fixed at the one end of the model, which illustrates that all number of nodes were restricted to move in any direction, making that end equivalent to the fixed lower jaw of UTM. On the other hand, the displacement of about 33 mm was applied on the other end

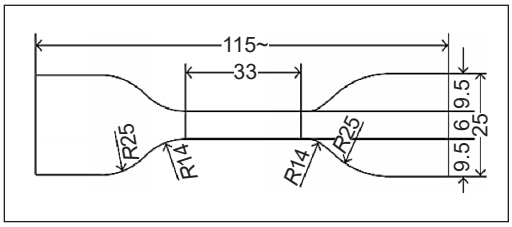

Figure 4. 3D model for PDMS material as per ASTM D412 type C standard
Note. Dimension unit in mm

of the model in the x-direction. There would be no displacement in the other two directions, i.e., the y and z directions were fixed ($U_y = U_z = 0$). The boundary conditions and meshing of the proposed parametrized FE model of PDMS material are depicted in Figure 5.

In the C3D8RH element type, the pressure or stress is considered an independent interpolated solution variable connected with displacement solution via constitutive theory (Shahzad et al., 2015). The mesh sensitivity analysis for the uniaxial tensile test was investigated upon establishing the FE model. This analysis aims to determine the ideal element size, type, and numerical formulation to get good results with the least computational work. Different mesh sizes, such as from 2 mm to 0.5 mm of linear formulation, were utilized to evaluate the stress-strain values of the PDMS model along the x-direction. The simulated stress-strain values were then compared with the experimental values to validate the best-fit hyper-elastic model with the respective mesh size. To determine the quality and convergence of mesh size for the simulated results with experimental data, the mean absolute error (*MAE*) against each mesh size (Martinez et al., 2018; Gómez et al., 2017; Lorza et al., 2017) was calculated using Equation 21.

$$MAE = \frac{1}{k}\sum_{m=1}^{k}\left|Y_{m,exp} - Y_{m,FE}\right| \quad [21]$$

Where k represents the total number of stress-strain data points with m = 1,2,3, ... , k integers. The experimental and FE stress values with m number of points are denoted by $Y_{m,exp}$, and $Y_{m,FE}$, respectively.

In addition, the mesh quality enhancement of different mesh sizes is a significant issue for various real-world problems. The results obtained after simulation can be affected by the analysis of the element quality of the mesh. There are variable methods used to improve the quality of mesh sizes, such as aspect ratio (Parthasarathy & Kodiyalam, 1991), Jacobean ratio, and maximum/minimum angles (Chen et al., 2003; Dassi et al., 2016; Ma & Wang, 2021). This research examined the aspect ratios of all the mesh sizes, i.e.,

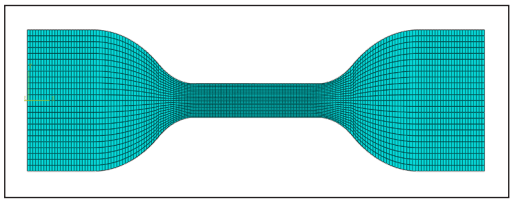

(a)

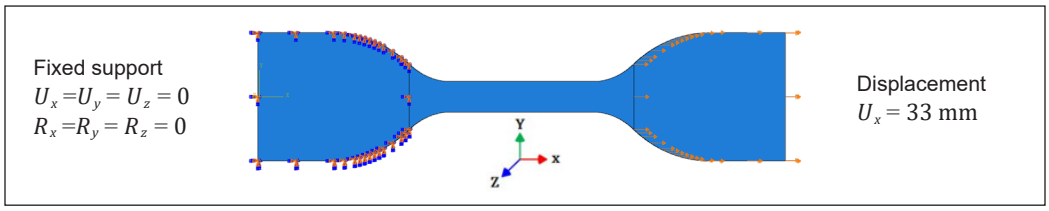

(b)

Figure 5. 3D dumbbell-shaped model of PDMS material: (a) Meshing; and (b) boundary conditions

from 2 mm to 0.5 mm, to determine the mesh quality factor. The aspect ratio is, however, defined as the ratio of the longest edge and the shortest normal dropped from a vertex to the opposite face of the element. A good quality mesh must possess an aspect ratio value of less than 5 for the majority of its elements, i.e., equal to or greater than 90% (SYSTEMES, 2021). The high aspect ratios are related to the greater discrepancies of the FE modeling and negatively influenced the convergence of the simulation results. Maintaining the ideal aspect ratio value of 1 for complicated geometries is impossible. Therefore, the modest values of aspect ratios can be retained in the crucial regions of the domain to ensure the fidelity of the simulated results. To highlight the elements with an aspect ratio larger than a certain value, the user must set a criterion in the Verify Mesh tool of Abaqus. Nonetheless, the two aspect ratios greater than 10 and greater than 3 were chosen for the mesh quality analysis of different mesh sizes of the PDMS material.

Besides, the simulated stress-strain values of the reduced polynomial hyper-elastic model were acquired in the natural logarithmic scale. The obtained stress-strain data were converted into engineering stress-strain using Equations 21 and 22 to compare with the experimental data. However, Table 4 shows the simulated engineering stress-strain values at different mesh sizes along with the respective number of nodes, elements, computational cost, aspect ratios, and MAE error.

$$\sigma^{true} = \sigma^{eng} e^{\varepsilon^{true}} = \sigma^{eng} (1 + \varepsilon^{eng}) \quad [21]$$

$$\varepsilon^{true} = \ln(1 + \varepsilon^{eng}) \quad [22]$$

The parameters in Equations 21 and 22 are as follows: σ^{true} gives the true stress values, σ^{eng} represents the engineering stress, and ε^{true} and ε^{eng} denote the true strain and engineering stress values, respectively.

It is worth noticing from Table 4 that by decreasing the mesh sizes from 2 mm to 0.5 mm, the number of nodes and elements increased, which provides the stress-strain simulated results very close to the experimental results. The accuracy of the results increased by increasing the number of nodes and elements, but the main purpose of meshing was to validate the stress-strain data of the best-fit hyper-elastic model with the experimental data. 0.6 mm and 0.5 mm mesh sizes possessed the lowest MAE of 0.049% than the other mesh sizes, but it is not enough to select the mesh size based on MAE only. Therefore, other factors such as aspect ratio and computational cost are also very important in choosing the best mesh size for PDMS material. For this purpose, 0.8 mm mesh size exhibited the lowest aspect ratio of 1.93 with the acceptable MAE (0.053%) and computational cost of 331 seconds. The maximum von Mises engineering stress and strain were obtained at 0.8 mm as 0.009890 MPa and 0.783718, respectively. Consequently, these simulated stress-strain values agree with the experimental stress (0.011140 MPa) and strain (0.78450). Based on

these results, a 0.8 mm mesh size of C3D8RH linear formulation was opted to validate the best-fit hyper-elastic model, i.e., reduced polynomial ($N = 6$). Thus, the contour plots of von Mises true stress and maximum principal true strain along x–the direction for the particular mesh size and element type are illustrated in Figure 6.

According to the contour plots, the maximum variation in stress and strain occurred at the necking of the 3D dumbbell-shaped model of the PDMS material because the boundary conditions with 33 mm gauge length, were applied simultaneously at the two ends of the sample, i.e., 33 mm displacement along x-direction at one end and all degree of freedom fixed on another end.

Table 4
Various mesh sizes with aspect ratio and mean absolute error of PDMS

Mesh Size (mm)	Nodes	Elements	Computational cost (sec)	Aspect Ratio	Max. von Mises engineering stress (MPa)	Max. principal engineering strain	*MAE* (%)
2.0	1026	448	27	2.23	0.009081	0.728519	0.082
1.8	1560	704	44	2.21	0.009154	0.733456	0.075
1.6	2064	935	56	2.01	0.009537	0.759615	0.063
1.4	2790	1288	71	2.15	0.009647	0.767076	0.061
1.2	3328	1545	78	2.29	0.009679	0.769281	0.060
1.0	6840	4284	215	2.18	0.009794	0.777118	0.058
0.8	10296	6510	331	1.93	0.009890	0.783718	0.053
0.7	12600	8016	419	1.99	0.009968	0.789038	0.053
0.6	24480	17661	1026	2.0	0.010043	0.794167	0.049
0.5	33740	24480	1870	1.94	0.010110	0.798581	0.049

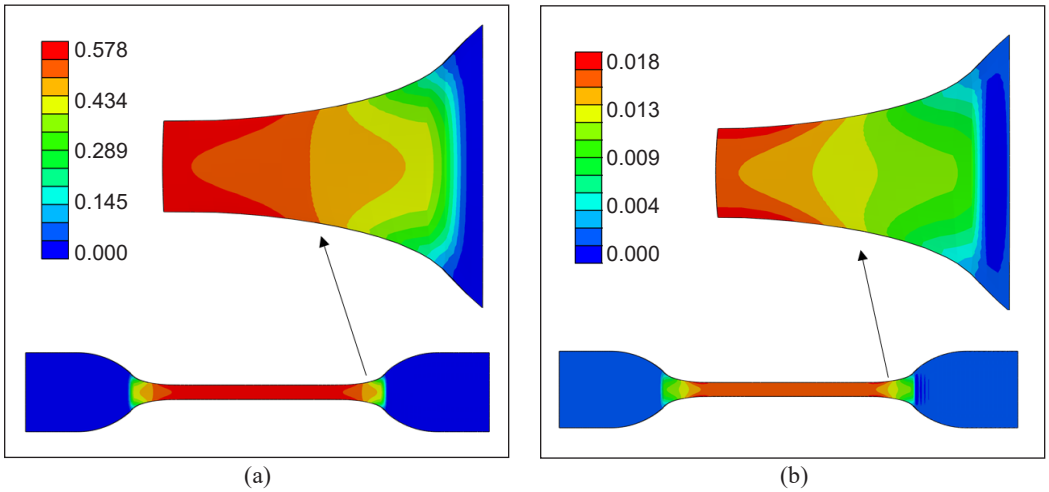

Figure 6. Contour plots of the Reduced Polynomial ($N = 6$) model: (a) Simulated true strain; and (b) simulated true stress

CONCLUSION

In this work, the mechanical behavior of PDMS was characterized through uniaxial tensile test and hyper-elastic material models. The uniaxial tensile test data obtained by UTM was imported into Abaqus, and curve fitting for different hyper-elastic material models was carried out. Among these hyper-elastic models, the reduced polynomial ($N = 6$) model was the most adequate solution for fitting the maximum points of experimental data according to the evaluation of the coefficient of determination (R^2) value of every hyper-elastic model. However, the reduced polynomial model exhibited the highest R^2 value (0.9963) than others. The FE simulation was then conducted on the PDMS sample to validate the reduced polynomial model. For this purpose, the analysis was carried out under the same boundary conditions as in the experimental analysis, i.e., fixed all DOF at one end, and 33 mm displacement was applied on the other end along the x-direction. The material constants of the best-fit hyper-elastic model were implemented on the 3D model. The simulation used different mesh sizes (2 mm to 0.5 mm) of C3D8RH linear formulation element type. The accuracy of the simulated results was improved by performing mesh quality analysis in terms of aspect ratio, and the MAE error of every mesh was also calculated. Based on these criteria, 0.8 mm mesh size possessed the lowest MAE error (0.053%) with 331 seconds computational cost and the lowest aspect ratio of about 1.93 than other mesh sizes. Consequently, the stress-strain data of the reduced polynomial model with 6 material constants agreed with the experimental stress-strain data points. Thus, this model can better fit the test and simulated data with the same boundary conditions. The results of numerical simulation might be different from experimental values if the displacement and thickness values of the material change.

ACKNOWLEDGEMENT

This paper is a part of a research project supported through Research University Grant 1001. PMEKANIK.8014067 and Short-Term Grant 304.PMEKANIK. 6315494 by Universiti Sains Malaysia (USM). The authors thank the Polymer Lab and Rubber Lab of the School of Materials and Mineral Resources Engineering, USM, for providing experimental services to pursue this study.

REFERENCES

Akther, F., Yakob, S. B., Nguyen, N. T., & Ta, H. T. (2020). Surface modification techniques for endothelial cell seeding in PDMS microfluidic devices. *Biosensors*, *10*(11), Article 182. https://doi.org/10.3390/bios10110182

Ali, A., Hosseini, M., & Sahari, B. B. (2010). A review of constitutive models for rubber-like materials. *American Journal of Engineering and Applied Sciences*, *3*(1), 232-239. https://doi.org/10.3844/ajeassp.2010.232.239

Anssari-Benam, A., & Bucchi, A. (2021). A generalised neo-Hookean strain energy function for application to the finite deformation of elastomers. *International Journal of Non-Linear Mechanics, 128*, Article 103626. https://doi.org/https://doi.org/10.1016/j.ijnonlinmec.2020.103626

ASTM D412-16. (2021). *Standard test methods for vulcanized rubber and thermoplastic elastomers-tension*. ASTM International. https://doi.org/10.1520/D0412-16R21

Aziz, N. A., Saad, A. A., Ahmad, Z., Zulfiqar, S., Ani, F. C., & Samsudin, Z. (2020). Chapter 8 - Stress analysis of stretchable conductive polymer for electronics circuit application. In A. S. H. Makhlouf & M. Aliofkhazraei (Eds.), *Handbook of Materials Failure Analysis* (pp. 205-224). Butterworth-Heinemann. https://doi.org/https://doi.org/10.1016/B978-0-08-101937-5.00008-7

Bashirzadeh, Y., Qian, S., & Maruthamuthu, V. (2018). Non-intrusive measurement of wall shear stress in flow channels. *Sensors and Actuators, A: Physical, 271*, 118-123. https://doi.org/10.1016/j.sna.2018.01.012

Beda, T. (2007). Modeling hyperelastic behavior of rubber: A novel invariant-based and a review of constitutive models. *Journal of Polymer Science, Part B: Polymer Physics, 45*(13), 1713-1732. https://doi.org/10.1002/polb.20928

Beda, T., & Chevalier, Y. (2003). Hybrid continuum model for large elastic deformation of rubber. *Journal of Applied Physics, 94*(4), 2701-2706. https://doi.org/10.1063/1.1586471

Bien-aimé, L. K. M., Blaise, B. B., & Beda, T. (2020). Characterization of hyperelastic deformation behavior of rubber-like materials. *SN Applied Sciences*, *2*(4), Article 648. https://doi.org/10.1007/s42452-020-2355-6

Boyce, M. C., & Arruda, E. M. (2000). Constitutive models of rubber elasticity: A review. *Rubber Chemistry and Technology, 73*(3), 504-523. https://doi.org/10.5254/1.3547602

Casanova-Moreno, J., To, J., Yang, C. W. T., Turner, R. F. B., Bizzotto, D., & Cheung, K. C. (2017). Fabricating devices with improved adhesion between PDMS and gold-patterned glass. *Sensors and Actuators, B: Chemical, 246*, 904-909. https://doi.org/10.1016/j.snb.2017.02.109

Chen, Z., Tristano, J. R., & Kwok, W. (2003, September 14-17). Combined laplacian and optimization-based smoothing for quadratic mixed surface meshes. In *Proceedings of the 12th International Meshing Roundtable, IMR 2003* (pp. 360-370). Santa Fe, New Mexico, USA.

Dassi, F., Kamenski, L., & Si, H. (2016). Tetrahedral mesh improvement using moving mesh smoothing and lazy searching flips. *Procedia Engineering, 163*, 302-314. https://doi.org/10.1016/j.proeng.2016.11.065

Doan, H. G. M., & Mertiny, P. (2020). Creep testing of thermoplastic fiber-reinforced polymer composite tubular coupons. *Materials, 13*(20), 1-17. https://doi.org/10.3390/ma13204637

Faghihi, S., Karimi, A., Jamadi, M., Imani, R., & Salarian, R. (2014). Graphene oxide/poly(acrylic acid)/gelatin nanocomposite hydrogel: Experimental and numerical validation of hyperelastic model. *Materials Science and Engineering C, 38*(1), 299-305. https://doi.org/10.1016/j.msec.2014.02.015

Gómez, F. S., Lorza, R. L., Bobadilla, M. C., & García, R. E. (2017). Improving the process of adjusting the parameters of finite element models of healthy human intervertebral discs by the multi-response surface method. *Materials*, *10*(10), Article 1116. https://doi.org/10.3390/ma10101116

Gonzalez, M., Axisa, F., Bulcke, M. Vanden, Brosteaux, D., Vandevelde, B., & Vanfleteren, J. (2008). Design of metal interconnects for stretchable electronic circuits. *Microelectronics Reliability, 48*(6), 825-832. https://doi.org/10.1016/j.microrel.2008.03.025

Guo, Z., & Sluys, L. J. (2006). Application of a new constitutive model for the description of rubber-like materials under monotonic loading. *International Journal of Solids and Structures, 43*(9), 2799-2819. https://doi.org/10.1016/j.ijsolstr.2005.06.026

Hassler, C., Boretius, T., & Stieglitz, T. (2011). Polymers for neural implants. *Journal of Polymer Science, Part B: Polymer Physics, 49*(1), 18-33. https://doi.org/10.1002/polb.22169

Íñiguez-Macedo, S., Lostado-Lorza, R., Escribano-García, R., & Martínez-Calvo, M. A. (2019). Finite element model updating combined with multi-response optimization for hyper-elastic materials characterization. *Materials*, *12*(7), Article 1019. https://doi.org/10.3390/ma12071019

Izdihar, K., Razak, H. R. A., Supion, N., Karim, M. K. A., Osman, N. H., & Norkhairunnisa, M. (2021). Structural, mechanical, and dielectric properties of polydimethylsiloxane and silicone elastomer for the fabrication of clinical-grade kidney phantom. *Applied Sciences, 11*(3), 1-13. https://doi.org/10.3390/app11031172

Jewkes, R., Burton, H. E., & Espino, D. M. (2018). Towards additive manufacture of functional, spline-based morphometric models of healthy and diseased coronary arteries: *In vitro* proof-of-concept using a porcine template. *Journal of Functional Biomaterials*, *9*(1), Article 15. https://doi.org/10.3390/jfb9010015

Ju, M. L., Jmal, H., Dupuis, R., & Aubry, E. (2014). A Comparison among polynomial model, reduced polynomial model and Ogden model for polyurethane foam. *Material Science and Engineering Technology II, 856*, 169-173. https://doi.org/10.4028/www.scientific.net/AMR.856.169

Kim, B., Lee, S. B., Lee, J., Cho, S., Park, H., Yeom, S., & Park, S. H. (2012). A comparison among Neo-Hookean model, Mooney-Rivlin model, and Ogden model for Chloroprene rubber. *International Journal of Precision Engineering and Manufacturing, 13*(5), 759-764. https://doi.org/10.1007/s12541-012-0099-y

López-Campos, J. A., Segade, A., Casarejos, E., Fernández, J. R., & Días, G. R. (2019). Hyperelastic characterization oriented to finite element applications using genetic algorithms. *Advances in Engineering Software, 133*, 52-59. https://doi.org/10.1016/j.advengsoft.2019.04.001

Lorza, R. L., Bobadilla, M. C., Calvo, M. Á. M., & Roldán, P. M. V. (2017). Residual stresses with time-independent cyclic plasticity in finite element analysis of welded joints. *Metals*, *7*(4), Article 136. https://doi.org/10.3390/met7040136

Ma, Y., & Wang, M. (2021). An efficient method to improve the quality of tetrahedron mesh with MFRC. *Scientific Reports*, *11*(1), Article 22802. https://doi.org/10.1038/s41598-021-02187-1

Martin, S., & Bhushan, B. (2017). Transparent, wear-resistant, superhydrophobic and superoleophobic poly(dimethylsiloxane) (PDMS) surfaces. *Journal of Colloid and Interface Science, 488*, 118-126. https://doi.org/10.1016/j.jcis.2016.10.094

Martinez, R. F., Lorza, R. L., Delgado, A. A. S., & Pullaguari, N. O. P. (2018). Optimizing presetting attributes by softcomputing techniques to improve tapered roller bearings working conditions. *Advances in Engineering Software, 123*, 13-24. https://doi.org/10.1016/j.advengsoft.2018.05.005

Martins, P., Peña, E., Calvo, B., Doblaré, M., Mascarenhas, T., Jorge, R. N., & Ferreira, A. (2010). Prediction of nonlinear elastic behaviour of vaginal tissue: Experimental results and model formulation. *Computer Methods in Biomechanics and Biomedical Engineering, 13*(3), 327-337. https://doi.org/10.1080/10255840903208197

Meissner, B., & Matějka, L. (2002). Comparison of recent rubber-elasticity theories with biaxial stress-strain data: The slip-link theory of Edwards and Vilgis. *Polymer, 43*(13), 3803-3809. https://doi.org/10.1016/S0032-3861(02)00150-7

Nunes, L. C. S. (2011). Mechanical characterization of hyperelastic polydimethylsiloxane by simple shear test. *Materials Science and Engineering: A, 528*(3), 1799-1804. https://doi.org/https://doi.org/10.1016/j.msea.2010.11.025

Parthasarathy, V. N., & Kodiyalam, S. (1991). A constrained optimization approach to finite element mesh smoothing. *Finite Elements in Analysis and Design, 9*(4), 309-320. https://doi.org/10.1016/0168-874X(91)90004-I

Pucci, E., & Saccomandi, G. (2002). A note on the gent model for rubber-like materials. *Rubber Chemistry and Technology, 75*(5), 839-851. https://doi.org/10.5254/1.3547687

Ribeiro, J., Fernandes, C. S., & Lima, R. (2018). Numerical simulation of hyperelastic behaviour in aneurysm models. *Lecture Notes in Computational Vision and Biomechanics, 27*, 937-944. https://doi.org/10.1007/978-3-319-68195-5_102

Roh, C., Lee, J., & Kang, C. K. (2016). Physical properties of PDMS (polydimethylsiloxane) microfluidic devices on fluid behaviors: Various diameters and shapes of periodically-embedded microstructures. *Materials*, *9*(10), Article 836. https://doi.org/10.3390/ma9100836

Sattarian, M., & Ghassemi, A. (2019). Identifying the poly methyl methacrylate behavior during free thermoforming using experimental tests and numerical simulation. *Journal of Theoretical and Applied Mechanics, 57*(4), 909-921. https://doi.org/10.15632/jtam-pl/112414

Shahzad, M., Kamran, A., Siddiqui, M. Z., & Farhan, M. (2015). Mechanical characterization and FE modelling of a hyperelastic material. *Materials Research, 18*(5), 918-924. https://doi.org/10.1590/1516-1439.320414

Souza, A., Marques, E., Balsa, C., & Ribeiro, J. (2020). Characterization of shear strain on PDMS: Numerical and experimental approaches. *Applied Sciences, 10*(9), Article 3322. https://doi.org/10.3390/app10093322

Subhani, P. M., & Kumar, R. K. (2009). A new stored energy function for rubber like materials for low strains. *Mechanics of Advanced Materials and Structures, 16*(5), 402-416. https://doi.org/10.1080/15376490902781167

Sugihardjo, H., Tavio, T., & Lesmana, Y. (2018). FE model of low grade rubber for modeling housing's low-cost rubber base isolators. *Civil Engineering Journal, 4*(1), 24-45. https://doi.org/10.28991/cej-030966

SYSTEMES, D. (2021). *Mesh Quality Checks*. DASSAULT SYSTEMES. https://help.solidworks.com/2021/english/SolidWorks/cworks/c_Mesh_Quality_Checks.htm#:~:text=A good-quality mesh has,Aspect ratio of all elements

Tansel, D. Z., Brenneman, J., Fedder, G. K., & Panat, R. (2020). Mechanical characterization of polydimethylsiloxane (PDMS) exposed to thermal histories up to 300 C in a vacuum environment. *Journal of Micromechanics and Microengineering*, *30*(6), Article 67001. https://doi.org/10.1088/1361-6439/ab82f4

Wineman, A. (2005). Some results for generalized neo-Hookean elastic materials. *International Journal of Non-Linear Mechanics, 40*(2), 271-279. https://doi.org/https://doi.org/10.1016/j.ijnonlinmec.2004.05.007

Wriggers, P. (2008). *Nonlinear Finite Element Methods*. Springer Berlin Heidelberg. https://doi.org/10.1007/978-3-540-71001-1

Xue, L., Pham, J. T., Iturri, J., & Del Campo, A. (2016). Stick-slip friction of PDMS surfaces for bioinspired adhesives. *Langmuir, 32*(10), 2428-2435. https://doi.org/10.1021/acs.langmuir.6b00513

Yu, Y. S., & Zhao, Y. P. (2009). Deformation of PDMS membrane and microcantilever by a water droplet: Comparison between Mooney-Rivlin and linear elastic constitutive models. *Journal of Colloid and Interface Science, 332*(2), 467-476. https://doi.org/10.1016/j.jcis.2008.12.054

Zulfiqar, S., Saad, A. A., Chek, M. W., Sharif, M. F. M., Samsudin, Z., & Ali, M. Y. T. (2020). Structural and random vibration analysis of LEDs conductive polymer interconnections. *IOP Conference Series: Materials Science and Engineering, 815*, Article 012003. https://doi.org/10.1088/1757-899X/815/1/012003

Zulfiqar, S, Saad, A. A., Ahmad, Z., Yusof, F., & Fakpan, K. (2022). Analysis and characterization of polydimethylsiloxane (PDMS) substrate by using uniaxial tensile test and Mooney-Rivlin Hyper-elastic model. *Journal of Advanced Manufacturing Technology, 16*(1), 61-72.

Zulfiqar, S., Saad, A. A., Ahmad, Z., Yusof, F., & Bachok, Z. (2021). Structural analysis and material characterization of silver conductive ink for stretchable electronics. *International Journal of Integrated Engineering, 13*(7), 128-135.